A novel weight coefficient calculation method for the real-time state monitoring of the lithium-ion battery packs under the complex current variation working conditions.

WANG, S.-L., FERNANDEZ, C. XIE, Z.-W., LI, X.-X., ZOU, C.-Y., LI, Q.

2019

Received: 29 July 2019 | Revised: 24 August 2019 | Accepted: 28 August 2019

DOI: 10.1002/ese3.478

RESEARCH ARTICLE

Energy Science & Engineering Open Access

A novel weight coefficient calculation method for the real-time state monitoring of the lithium-ion battery packs under the complex current variation working conditions

Shun-Li Wang[1] | **Carlos Fernandez**[2] | **Zheng-Wei Xie**[3] | **Xiao-Xia Li**[1] | **Chuan-Yun Zou**[1] | **Qiang Li**[1]

[1]School of Information Engineering & Robot Technology Used for Special Environment Key Laboratory of Sichuan Province, Southwest University of Science and Technology, Mianyang, China

[2]School of Pharmacy and Life Sciences, Robert Gordon University, Aberdeen, UK

[3]Chengdu Institute of Organic Chemistry, Chinese Academy of Sciences, Chengdu, China

Correspondence
Shun-Li Wang, School of Information Engineering & Robot Technology Used for Special Environment Key Laboratory of Sichuan Province, Southwest University of Science and Technology, Mianyang 621010, China.
Email: wangshunli@swust.edu.cn

Funding information
National Natural Science Foundation of China, Grant/Award Number: 61801407; China Scholarship Council, Grant/Award Number: 201908515099; Sichuan Province Science and Technology Support Program, Grant/Award Number: 19ZDYF1098, 2018GZ0390, 2019JDTD0019 and 2019YFG0427; Scientific Research Fund of Sichuan, Grant/Award Number: 17ZB0453; Teaching Research Project, Grant/Award Number: 18lzx665, 18gjzx11 and 18xnsu12

Abstract

A novel real-time state monitoring method is proposed to realize the real-time energy management of the lithium-ion battery packs, which is conducted in the iterative computational calculation process by introducing an improved weighting factor-unscented Kalman filtering algorithm. The accurate state monitoring treatment is investigated by applying a new iterate calculation thought, in which the improved weight coefficient parameter is constructed and its numerical stability is improved. Meanwhile, the recursive calculation is derived by using the real-time measured factors, according to which the state-of-charge estimation is realized accurately. Aiming to adapt the complex current variation working conditions, the nonlinear treatment is introduced to construct the mathematical unscented transforming function. As can be known from the experimental results, the state-of-charge estimation accuracy is 98.34% under the complex current charge-discharge working conditions. Meanwhile, the effective closed-circuit voltage trackage is also investigated accurately and its tracking error is within 3.51% in the complex working conditions, which provides a good security guarantee for the reliable energy supply of the lithium-ion battery packs.

KEYWORDS

complex current variation, Kalman filter, lithium-ion battery, state monitoring, unscented transform, weight coefficient

1 | INTRODUCTION

The lithium-ion battery has some attracting advantages over other rechargeable batteries, such as high energy density, stable voltage, and eco-friendly. The high energy density is required in the power supply application of the new energy vehicle, unmanned aerial vehicle, and energy storage system. As a result, the lithium-ion battery packs can be applied as the power source, which is also taken as the auxiliary power for the energy shortages and other sudden emergencies.[1] Because of the positive correlation relationship between the energy consumption and the weight of the flying objects, the energy density is chosen as an important indicator of its power supply systems. Therefore, the lithium-ion battery pack has become the power supply trend of the unmanned aerial vehicles.[2] However, the cumulative working state estimation error restricts the power promotion of the lithium-ion battery pack severely, according to which the state-of-charge estimation researches are investigated extensively.[3] The effective implementation was established with the charge replacement, in which the extended Kalman filtering algorithm was introduced and realized.[4] The online battery impedance measurement method was also studied by using the direct current-direct current conversion together with its power converter control.[5] A systematic and reliable state-of-charge estimation method was proposed for the lithium-ion battery pack by using the comprehensive state evaluation algorithm.[6] The recovery strategy was studied for the lithium-ion batteries on the aging characteristics at high temperature conditions,[7] and the direct measurements were investigated by using the diffusive coefficients of the lithium-ion batteries.[8] The state-of-charge inconsistency evaluation was implemented for the lithium-ion battery pack by using the mean differential model and the extended Kalman filtering algorithm.[9] The incremental capacity and differential voltage were analyzed for the state-of-charge estimation of the lithium-ion batteries,[10] and a new multi-time-scale filter was proposed to obtain the state of energy and the state of power values.[11] The state of health diagnosis was realized according to the surface temperature changes.[12] The related research provides scientific and technological references to the state-of-charge estimation of the lithium-ion battery together with its energy management. However, there is still a lack of effective technical solutions to realize the real-time working state monitoring of the lithium-ion battery pack.

The lithium-ion battery can be implemented in the electric vehicles together with the battery management by using the active current control algorithm.[13] A joint state-of-charge estimation was performed for the electric vehicle power batteries by using the least square and Kalman filter algorithms,[14] and an online frequency tracking algorithm was proposed by using the closed-circuit voltage spectroscopy to realize the optimal charging maintenance of the lithium-ion batteries.[15] The performance evaluation of the modular equalization system was also performed,[16] and a new thermal coupling model was built for the state-of-charge estimation.[17] A real-time state-of-charge estimation was investigated by using the fad Kalman filter algorithm for the lithium-ion batteries,[18] and the multimodel estimation was realized by using the H-infinity algorithm.[19] A new modeling method was proposed by Liu et al,[20] and the energy preheating strategy was discussed for the lithium-ion batteries together with its latency temperature.[21] The path dependence was studied by using the aging characteristics at different storage conditions,[22] and the working state estimation was realized for the lithium-ion batteries by using the extended Kalman filtering algorithm together with the physicochemical model.[23] A realistic life prediction was investigated,[24] and the wavelet-based state-of-charge estimation was conducted for the lithium-ion batteries. The memory effect was investigated [25] for the large format lithium-ion batteries, and the data-driven model [26] was used to perform the robust capacity estimation in its management system.[27] The online equalizing strategy was conducted for the lithium-ion battery packs [28] by considering the state of balance conditions among the internal connected battery cells. The online battery parameter identification was performed for the equivalent circuit model by using the decoupling least square technique.[29] An improved online state-of-charge estimation algorithm was proposed by using the adaptive cubature Kalman filter processing treatment,[30] which was also realized by using the dual scale adaptive particle filter,[31] and the improved state-of-charge determination was conducted by using the genetic algorithm as well.[32]

In order to realize the real-time parameter monitoring, the fault-tolerant voltage measurement should be investigated for the series-connected lithium-ion battery packs and the state-of-charge estimation was also realized by using the fractional and integral order methods.[33] The state-of-charge estimation was conducted by using the H-infinity observer,[34] in which the hysteresis characteristic was also considered. The modeling and state-of-charge prediction were conducted for the lithium-ion battery and ultracapacitor hybrids with a co-estimator,[35] and its degradation behavior [36] was studied during its aging process by considering the internal resistance increment characteristics.[37] The effective implementation of charge replacement was also conducted in the hybrid electrical energy storage system.[38] The relationship of coulomb efficiency and energy decrease was studied,[39] and the extended Kalman filtering-based materialization model was built by using the charge curve [40] to construct a new Gaussian processing regression model. The probability-based remaining capacity estimation was investigated by using the data-driven and neural network models.[41] The hierarchical message was used to describe the degradation characteristics,[42] and the sampling diagnosis was studied for the lithium-ion batteries.[43] A state recognition method is proposed to identify

the degradation by using the electrochemical model for all climate working environments.[44] The online state-of-charge estimation [45] was performed by using the multimodel data fusion method,[46] and the parameter sensitivity was performed on the lithium-ion battery modeling.[47]

In order to improve the state-of-charge estimation accuracy, a novel weighting factor-unscented Kalman filter (WF-UKF) calculation method is proposed to realize the real-time state monitoring of the lithium-ion battery packs in the complex current variation working conditions. It is realized mainly by using the real-time parameter identification and correction, the estimation process of which is treated as a black-box module. Then, the iterative calculation based on the proposed WF-UKF algorithm is performed to obtain the state-of-charge values at various operating conditions, according to which the online parameter identification and state-of-charge estimation are conducted by using the forgetting factor recursive least square and nonlinear Kalman filter algorithms. Meanwhile, the state-space description is investigated along with the noninteger order derivatives. Considering the temperature effects, the Peukert equation is introduced into the iterate calculation process, according to which the estimator is investigated by considering the temperature effect, hysteresis potential, and thermal evolution of the lithium-ion battery packs.

2 | MATHEMATICAL ANALYSIS

The mathematical state-of-charge estimation method is studied for the lithium-ion battery packs, in which the comprehensive state evaluation is introduced into the iterative calculation process combined with the state-space description and parameter identification of the equivalent circuit models. According to the improved WF-UKF approach, the battery energy state is estimated real-timely in the associated battery management system for the security protection, realizing the energy state management purpose of the lithium-ion battery packs.

2.1 | State-space description

The mathematical description is conducted for the lithium-ion battery packs, in which the series-connected power source and resistance are introduced along with the electro-motive force. In order to characterize the inconsistency effect among the internal connected battery cells, the operational characteristic description is investigated for the lithium-ion battery pack, making it to be performed accurately. The working characteristics of the lithium-ion battery can be expressed accurately in the improved modeling treatment, which realizes the model framework construction. In addition, the equivalent model is analyzed by the experimental test together with its parameter identification. In order to realize the inconsistency characterization of the serially connected lithium-ion battery packs, a time-varying voltage source is introduced along with the open circuit voltage source parameter U_{oc}. The closed-circuit voltage is measured in real time when the positive and negative terminals of the lithium-ion battery pack are connected to the external circuit components during the charge-discharge operation time period. When the lithium-ion battery pack is in the charge-discharge working state, the functional relationship can be obtained for the state-space mathematical expression that can be used in the iterate calculation process, in which the state equation can be obtained as shown in Equation (1).

$$U_L(t) = E(t) - U_p(t) - R_o(t)\, I(t) \tag{1}$$

In the above expression, $E(t)$ is the ideal power source and R_o is the ohmic internal resistance to the coulomb efficiency. R_p and C_p are the polarization internal resistance and capacitance, which are used to express the dynamic characteristics of the lithium-ion battery pack. $I(t)$ is introduced to describe the current, and U_p is used to characterize the voltage at both ends of the parallel resistance-capacitance loop circuit, the calculation process of which can be described mathematically as shown in Equation (2).

$$\widehat{U}_p(t) = -\frac{1}{R_p(t)\, C_p(t)} U_p(t) + \frac{1}{C_p(t)} I(t) \tag{2}$$

After obtaining the voltage and current data onto the parameter identification experiments with different state-of-charge levels, the multivariate linear regression is introduced to identify the parameters of the equivalent circuit model. The identification treatment is investigated to obtain the relationship between the polarization current and the linearized load current of the circuit equation, which is described as shown in Equation (3).

$$\begin{cases} U_L(t) = E(t) - U_p(t) - R_o(t)\, I_L(t) \\ I_p(t) = \left[1 - \dfrac{1 - e^{-\frac{T}{\tau}}}{\frac{T}{\tau}}\right] I_L(t) + \left[1 - \dfrac{1 - e^{-\frac{T}{\tau}}}{\frac{T}{\tau}} - e^{-\frac{T}{\tau}}\right] I_L(t-1) + e^{-\frac{T}{\tau}} I_p(t-1) \end{cases} \tag{3}$$

Wherein, T is the segmentation time of the linear processing, which represents the parameter sampling time of the battery management system. $I_p(t)$ is used to describe the current flowing through the polarization capacitance. $I_L(t)$ is used to describe the current flowing through the electrical loads. Then, the subsequent calculation framework can be established, which is introduced into the model parameter identification. Afterward, the equivalent model and its state-space equation can be established for the lithium-ion

battery pack, in which the data acquisition and processing treatment are transformed into the discrete time forms of the computerized real-time calculation. By conducting the state-space representation, the mathematical description of the equivalent model can be conducted for the lithium-ion battery pack. Combined with the Ampere-hour integration method, the parameters of S and U_p are used as the state variables and the linearized state-space equation can be obtained that are shown in Equation (4).

$$\begin{bmatrix} U_p(k) \\ S(k) \end{bmatrix} = \begin{bmatrix} 1-\frac{T}{R_pC_p} & 0 \\ 0 & 1 \end{bmatrix} \begin{bmatrix} U_p(k-1) \\ S(k-1) \end{bmatrix} + \begin{bmatrix} U_L(k) & 0 \\ 0 & I(k) \end{bmatrix} \begin{bmatrix} \frac{T}{C_p} \\ -\frac{\eta T}{C_p} \end{bmatrix} + \begin{bmatrix} w_1(k-1) \\ w_2(k-1) \end{bmatrix} \tag{4}$$

The parameter significances are described as follows: k (time point), S (state of charge), $U_L(k)$ (closed-circuit voltage value), R_o (ohm resistance), $I(k)$ (output current), T (parameter detection time period). By investigating the circuit analysis, the state-space equation can be described accurately toward the circuit structure. When the lithium-ion battery pack is in an open circuit state for about 40 minutes as the internal reaction of the battery is stable, U_{OC} equals to the closed-circuit voltage value which can be described as $U_{OC} = U_L$. After that, the observation equation can be transformed in conjunction with the equivalent circuit model by selecting the closed-circuit voltage as the observation parameter, according to which the transformation can be obtained by Equation (5).

$$\left[U_L(k)\right] = \left[E(k)\right] - \begin{bmatrix} 1 & 0 \end{bmatrix} \begin{bmatrix} U_p(k) \\ S(k) \end{bmatrix} - \left[R_o\right]\left[I_L(k)\right] + v(k) \tag{5}$$

There are some parameters that should be known in the above expression: E (open circuit voltage), R_o (ohm resistance), U_L (closed-circuit voltage), w_1 and w_2 (process noise), v (observation noise). In order to obtain the parameter value of U_p, the calculation process of τ is set as $\tau = R_pC_p$. When using the WF-UKF algorithm for the state estimation of the lithium-ion battery pack, it is required to establish an observation equation for the estimated state of charge and the output vector U_L. According to the identified parameter data, the relationship between R_p, E, and S is fitted, respectively, for the charge-discharge directions, and then, the matrix required for the improved Kalman filter calculating treatment is defined as shown in Equation (6).

$$\begin{aligned} X(k) &= \begin{bmatrix} U_p(k) \\ S(k) \end{bmatrix} \quad A(k) = \begin{bmatrix} 1-\frac{T}{R_pC_p} & 0 \\ 0 & 1 \end{bmatrix} \\ B(k) &= \begin{bmatrix} \frac{T}{C_p} \\ -\frac{\eta T}{C_p} \end{bmatrix} \quad C(k) = \frac{\partial U_L}{\partial X} = \begin{bmatrix} \frac{\partial U_L}{\partial U_p} & \frac{\partial U_L}{\partial S} \end{bmatrix} \end{aligned} \tag{6}$$

In the above expression, $S(k)$ is used to represent the state-of-charge value at the time point of k. The calculation expression of $U_p(k)$ can be substituted for the mathematical calculation process of $U_L(t)$, which can be discretized to obtain the final observing equation. The mathematical relationship can be characterized by using the initial treatment and real-time calculation that are shown in Equation (7).

$$\frac{\partial U_L}{\partial U_p} = 1, \frac{\partial U_L}{\partial S} = \frac{\partial E}{\partial S} + I_L\frac{\partial R_o}{\partial S} \tag{7}$$

The proposed mathematical model provides a great feasibility for the rapid recognition result analysis, according to which the state-space equation can be obtained. The general knowledge of covariance and noise is taken as the priory known condition, in which the additional considerations can be made in the dependent submodules. By investigating its internal working state monitoring structure, the application characterization can be realized and the operating characteristics can be obtained through the experiments. Combined with the battery management system design, the working characteristics are analyzed to realize the parameter identification process, according to which the model coefficients can be obtained.

2.2 | Iterative correction algorithm

The iterative calculation is investigated to realize the state-of-charge estimation of the power lithium-ion battery pack, which utilizes the experimental results and the model parameter identification mechanism. In order to obtain its state-space function, the comprehensive evaluation is introduced into the mathematical calculation process. An improved WF-UKF-based state-of-charge estimation method is implemented together with the recalibrating process of the Ampere-hour counter as it is simple and easy to be realized. In order to obtain the input factors of the state-of-charge estimation model, the parameter identification submodule is established. Finally, the iterate calculation process is performed in conjunction with the balance state impact correction. In this way, the state-of-charge estimation of the associated battery management system can be realized and the iterative calculation of the proposed method can be implemented.

The state and observation equations of the linearization are like the Kalman filtering equations[48] in the pretreatment process, in which the initial value of the covariance matrix can be obtained by calculating the desired variance in the initial error correction process. Furthermore, the state-of-charge estimation model structure can be constructed by the operating characteristic analysis of the lithium-ion battery pack, in which $U_L(k)$ is the observing closed-circuit voltage value and the state-of-charge value can be initialized. The input parameters of the state-space equation can be obtained by the

real-time monitoring, in which $U_L(k)$ is the output parameter of the observation equation and the calculation process is shown as follows.

2.2.1 | S1: Prediction

1. The initial working state can be obtained by conducting the predicted calculation treatment. In the front of each iteration treatment, the state-of-charge value is set as $S = S(k\text{-}1)$ to calculate its predictive value, the calculation process of which is shown in Equation (8).

$$S(k|k-1)=A(k-1)S(k-1)+B(k-1)I_L(k) \tag{8}$$

2. The priory covariance error of the working state estimation is expressed in Equation (9).

$$P(k|k-1)=A(k-1)P(k-1)[A(k-1)]^T+\Gamma(k-1)Q_w[\Gamma(k-1)]^T T \tag{9}$$

2.2.2 | S2: Correction

1. The Kalman gain can be obtained by the calculation treatment that is shown in Equation (10).

$$K(k)=P(k|k-1)[C(k)]^T\left[C(k)P(k|k-1)[C(k)]^T+\frac{R(k)}{T}\right] \tag{10}$$

2. The updated state value considering the observed data can be obtained by investigating the calculation process that is shown in Equation (11).

$$\begin{cases} U_L(k)=E(k)+R_o(k)I_L(k)+U_p(k) \\ X(k)=X(k|k-1)+K(k)\left[Y(k)-U_L(k)\right] \end{cases} \tag{11}$$

3. The covariance error matrix of the state-of-charge estimation can be corrected by the mathematical treatment that is shown in Equation (12).

$$P(k)=[I-K(k)C(k)]P(k|k-1) \tag{12}$$

As can be known from the equivalent model and the experimental results, the sampling data points can be obtained by conducting the unscented transform treatment, which is investigated by the calculation process of the prior mean and variance factors. Then, it is applied to the state-space mathematical description and the state-of-charge estimation process, according to which the $2n + 1$-dimensional Sigma data set can be obtained by the following unscented transform calculations together with its weight coefficients. Thereafter, its characteristics can be obtained which are shown in Equation (13).

$$\begin{cases} X^{(i)}=\overline{X}, i=0; X^{(i)}=\overline{X}+\left(\sqrt{(n+\lambda)P}\right)_i, i=1,\cdots,n \\ X^{(i)}=\overline{X}-\left(\sqrt{(n+\lambda)P}\right)_i, i=n+1,\cdots,2n \end{cases} \tag{13}$$

In the above expression, i is used to represent the i-th column of the sampling data sequence and its covariance matrix. P is the product of its transposed and arithmetic square root parameters that are shown in Equation (14).

$$\left(\sqrt{P}\right)^T\left(\sqrt{P}\right)=P \tag{14}$$

The battery data point set can be obtained by using the original distribution together with its state screening spectrum, which is replaced by using the nonlinear state equation and the observation equation. Afterward, their mean and variance values can be analyzed by using these data points, the accuracy of which can reach the second order without conducting the linearization treatment. The weight coefficient of the sampling data sequence can be implemented by Equation (15).

$$\begin{cases} \omega_m^{(0)}=\dfrac{\lambda}{n+\lambda}, \lambda=\alpha^2(n+\kappa)-n \\ \omega_c^{(0)}=\dfrac{\lambda}{n+\lambda}+\left(1-\alpha^2+\beta\right) \\ \omega_m^{(i)}=\omega_c^{(i)}=\dfrac{1}{2(n+\lambda)}, i=1,\cdots,2n \end{cases} \tag{15}$$

In the above expression, the subscript parameter m represents the average value of the Sigma data point set and the subscript c is used to characterize the variance between the Sigma data point set. The superscript i indicates the serial number of the sampling data points. λ defines the overall scaling parameter, which can be adjusted by the parameter correction treatment to reduce the overall state-of-charge estimation error. The choice of α determines the state distribution that is relative to the state-of-charge data sequence. Furthermore, $(n + \lambda)P$ is set as a semipositive matrix, and then, the value of κ can be obtained. By selecting the non-negative weight coefficient parameter β, the statistical high-order term error of the state-space equation

is integrated to ensure the effective unscented transform influence.

2.3 | Double unscented transform

Aiming to realize the computational reduction purpose, the three-particle mode is designed and applied for the iterative calculation. In order to realize the one-step state-of-charge predicting calculation, a simplified unscented transform treatment is investigated to realize the nonlinear mean and variance conversion. Wherein, the sampling data sequence set is also used to approximate the posterior probability density, in which the Jacobian matrix calculation is not necessary to be conducted. Therefore, there is no neglected high-order term discarding treatment for the calculation process,[49] making the statistical feature has the higher precision advantage. As a result, the nonlinear error can be reduced effectively for the working state estimation. By conducting the three-particle unscented transform treatment, the data averaging calculation is performed by using two weighting treatments of the Sigma points.

The three Sigma state-of-charge data point sequence can be obtained by the first unscented transform treatment, together with the weight parameters of w_c and w_m, respectively. Then, the predicted values can be obtained by the state equation corresponding to these data points. Meanwhile, the one-dimensional predicted state-of-charge value can be calculated by combining the weighted summation for these three time-updating state-of-charge values. Afterward, the unscented transform treatment is performed again on the predicted state-of-charge result, in which the transformation is applied to the observation equation. In this way, three predictive closed-circuit voltage values can be obtained, which are used in the correction step to improve the state-of-charge estimation accuracy. Afterward, the predicted value can be obtained by the weighting treatment, which is used as the state update link in the iterate calculation process.

The state-of-charge estimation of different time points includes the random state variable, which is fused with the white Gaussian noise $w(k)$. Meanwhile, the observed random variable $U_L(k)$ is fused by the white Gaussian noise $v(k)$.[48] Among them, $f(*)$ is a nonlinear equation of the state-space function and $g(*)$ is the nonlinear observational equation that describes the closed-circuit voltage characteristics. Furthermore, the variance of the noise matrix $w(k)$ is described by using the symbol Q and the variance of the noise matrix $v(k)$ is described by using the symbol R. Considering these random noise influences, the state-of-charge estimation can be realized for the lithium-ion battery pack at different time points.

A series of weighted Sigma data point selection can be investigated to realize the mean value estimation of the data samples. By conducting this iterative calculation, the double unscented transform treatment and the improved WF-UKF algorithm can be implemented in the state-of-charge estimation process of the lithium-ion battery pack. And then, the measurement equation can be realized that describes the closed-circuit voltage and the state-of-charge observation. The iterate calculation lies on the handling treatment of the real-time detected parameters, in which no complex mathematical models must be derived and investigated, making the fast error analysis in each prediction and correction step to be possible.

2.4 | Weight coefficient calculation

The WF-UKF approach is an extension of the basic Kalman filter algorithm with the high precision and robustness advantages, which also relies on the accurate mathematical models by using the statistical features of the process and observation noise. In the state-of-charge estimation process of the power lithium-ion battery pack, the statistical characteristics of the process and the observed noises change significantly as well when the operating environment and the motion state change drastically, which will reduce the accuracy and stability of the conventional WF-UKF algorithm. If the conventional calculation algorithm is used in the state-of-charge estimation process directly, the estimation result may encounter a covariance negative decision problem of the later stage operation due to the severe current variation. And then, the covariance P_k becomes a negative value. However, the Cholesky decomposition requires that the matrix has the semidefiniteness characteristic. Otherwise, the iterate calculation may lead to diverge which is invalidating for the state-of-charge estimation process, the reason of which is that there is a rounding error in the numerical calculation process.

In order to improve the numerical instability of the WF-UKF algorithm, the covariance encounters the later operation that is determined negatively, which may lead to the state-of-charge estimation failure. The QR decomposition is introduced into the WF-UKF-based state-of-charge estimation process, in which the square root of the state variable covariance is used in the unscented transform treatment instead of the covariance. The iterative operations are performed to ensure the non-negative qualitative and numerical stability of the covariance matrix. As a result, the square root of the error covariance can be used instead of the error covariance to participate in the operation process, and the square root of the covariance is directly transmitted into the state-of-charge estimation process of each calculation step to avoid the redecomposition phenomena. When S is used to characterize the square root of the covariance matrix P (ie, $SS^T = P$), it can be guaranteed that P has the non-negative qualitative feature if $S \neq 0$. The iterate calculation process can be described as follows.

2.4.1 | Parameter initialization

The initial state variable value of *state of charge*$_0$ should be determined together with the initial value of the error covariance P_0. Among them, S_0 is the Cholesky factor of the covariance P_0, the initial value of which is determined by the mathematical description that is shown in Equation (16).

$$\begin{cases} \overline{X}_0 = E\left(X_0\right) \\ P_0 = E\left[\left(X_0 - \overline{X}_0\right)\left(X_0 - \overline{X}_0\right)^T\right] \\ S_0 = chol\left(P_0\right) \end{cases} \tag{16}$$

2.4.2 | Three-particle calculation

The Sigma pointed acquisition data onto state of charge can be obtained by conducting the unscented transform treatment that is shown in Equation (17).

$$\begin{cases} X(k-1)^{(i)} = \overline{X}(k-1), i = 0 \\ X(k-1)^{(i)} = \overline{X}(k-1) + \sqrt{(n+\lambda)}S(k-1)^i, i = 1, \cdots, n \\ X(k-1)^{(i)} = \overline{X}(k-1) - \sqrt{(n+\lambda)}S(k-1)^{i-n}, i = n+1, \cdots, 2n \end{cases} \tag{17}$$

In the above expression, S_k^i represents the i-th column of the Cholesky factor that characterizes the state variable covariance at k time point.

2.4.3 | One-step prediction

The time-updated state variable of state of charge in one-step prediction can be realized by using the state equation that is based on the state variable of state of charge at k-1 time point, according to which the input parameter values can be obtained. The calculation formula for the state-of-charge prediction process is shown in Equation (18).

$$X(k|k-1)^i = f\left\{X(k-1)^i, u(k-1)\right\} \tag{18}$$

The weighted average calculation process is shown in Equation (19).

$$\overline{X}(k|k-1) = \sum_{i=0}^{2n} \omega_m^i X(k|k-1)^i \tag{19}$$

Then, the QR decomposition is performed on the error covariance of the predicted state-of-charge value according to the one-step prediction of the state of charge at the sampling time point,[50] the calculation process of which is shown in Equation (20).

$$S_{X(k)}^- = qr\left\{\sqrt{\omega_c^{1:2n}}\left[X(k|k-1)^{1:2n} - \hat{X}(k|k-1)\right], \sqrt{Q(k)}\right\} \tag{20}$$

Considering that the values of α and k may generate the negative values of ω_c^0, Equation (21) is used to guarantee the semidefiniteness of the matrix.

$$S_{X(k)} = \text{cholupdate}\left\{S_{X(k)}^-, \sqrt{abs\left(\omega_c^0\right)}\left[X(k|k-1)^0 - \hat{X}(k|k-1)\right], \text{sign}\left(\omega_c^0\right)\right\} \tag{21}$$

Wherein, $S_{X(k)}$ represents the square root update of the error covariance for the working state value at k time point. According to the three-one-step state-of-charge prediction results, the observed closed-circuit voltage values can be obtained by using the observation equation correspondingly. Meanwhile, $S_{UL(k)}$ is used to represent the updated square root of the covariance for the observed variable U_L at k time point, the statistical characteristics are shown in the Equation (22).

$$U_L(k|k-1)^i = h\left\{X(k|k-1)^i, u(k)\right\} \tag{22}$$

The weighted average calculation process of U_L is shown in Equation (23).

$$\hat{U}_L(k|k-1) = \sum_{i=0}^{2n} \omega_m^i U_L(k|k-1)^i \tag{23}$$

The QR decomposition is shown in Equation (24).

$$S_{U_L(k)}^- = qr\left\{\sqrt{\omega_c^{1:2n}}\left[U_L(k|k-1)^{1:2n} - \hat{U}_L(k|k-1)\right], \sqrt{R(k)}\right\} \tag{24}$$

The decomposition calculation can be realized by using the function of cholupdate(*) as shown in Equation (25).

$$S_{U_L(k)} = \text{cholupdate}\left\{S_{U_L(k)^-}, \sqrt{abs\left(\omega_c^0\right)}\left[U_L(k|k-1)^0 - \hat{U}_L(k|k-1)\right], \text{sign}\left(\omega_c^0\right)\right\} \tag{25}$$

2.4.4 | Real-time correction

The updated state calculation process should be conducted by using the predicted state-of-charge value, in which the real-time closed-circuit voltage monitoring is conducted and is used for the correction treatment by multiplying the Kalman gain. The cross-covariance of the state and observed variables can be calculated accordingly, the value of which affects the magnitude of the KF gain directly. The covariance of these two parameters can be calculated by the summation calculation that is shown in Equation (26).

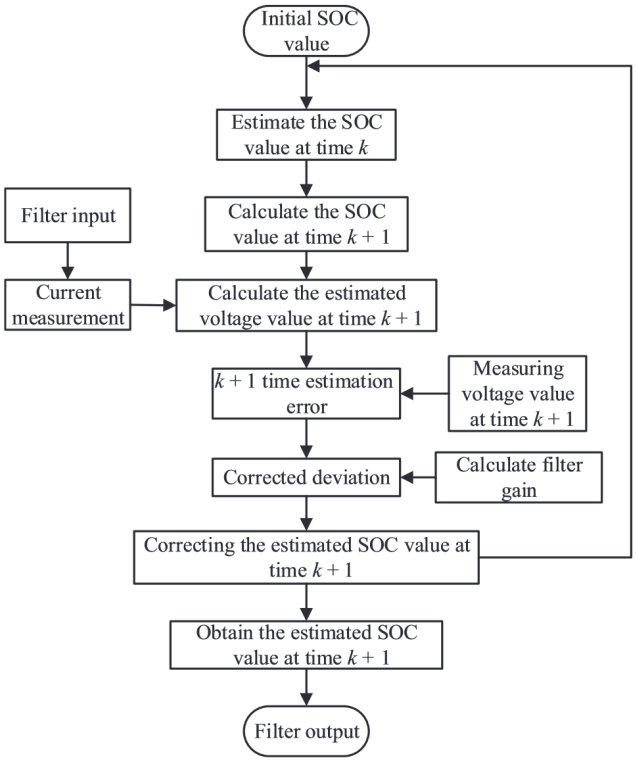

FIGURE 1 The estimation algorithm flowchart

$$P_{X(k)U_L(k)}=\sum_{i=0}^{2n}\omega_c^i\left[X(k|k-1)^i-\hat{X}(k|k-1)\right]\left[U_L(k|k-1)^i-\hat{U}_L(k|k-1)\right] \tag{26}$$

The accuracy of the Kalman gain will affect the state-of-charge estimation effect, which can be obtained because of the above formula.[51] By investigating the parameter solving process, the mathematical expression can be obtained for the Kalman gain calculation, which is described in Equation (27).

$$K(k)=P_{X(k)U_L(k)}\left[S_{U_L(k)}S_{U_L(k)}^T\right]^{-1} \tag{27}$$

Furthermore, the working state value of the k time point and its updating covariance error treatment can be conducted, in which $U_L(k)$ is the measured closed-circuit voltage value of the k time point. The updated state calculation process can be investigated and is shown in Equation (28).

$$\begin{cases} X(k)=\hat{X}(k|k-1)+K(k)\left[U_L(k)-\hat{U}_L(k|k-1)\right] \\ S(k)=\text{cholupdate}\left\{S_{X(k)^-},K(k)S_{U_L(k)},-1\right\} \end{cases} \tag{28}$$

In the optimized calculation process, the initial value is calculated by the Cholesky factorization and the square root of the covariance matrix. In the subsequent iterative calculation process, the updated factor directly forms the Sigma data point set. The time-updated factor of $S_{X(k)}^-$ is implemented by using the square root complex matrix, which contains the weighted Sigma points and superimposed process noise covariance. Then, the update treatment can be expanded combined with the QR decomposition. The optimization realizes the $P_{X(k|k-1)}$ updated treatment of the WF-UKF-based calculation process, which overcomes the shortcomings of poor stability and ensures the semidefiniteness of the covariance matrix.

2.5 | Estimation model realization

The general knowledge about covariance and noise is used as the prior knowledge, in which the current dependency should be also considered for the reliable state-of-charge estimation. The Hybrid Pulse Power Characterization experimental test is used for the parameter identification of the equivalent model, in which the mathematical function can be encapsulated in the separate *M* files. Then, the state-of-charge correction process takes the voltage and current parameters into account, by which the battery operating state information can be obtained to achieve the comprehensive state-of-charge estimation. The real-time monitoring of the state-of-charge values can be achieved by comparing the estimated state-of-charge value of the experimental result obtained by the Ah integral calculation. Then, the parameter values are constantly adjusted by the variance analysis to optimize the state-of-charge estimation model, which uses the WF-UKF algorithm and incorporates the nondestructive treatment in front of the state-of-charge estimation process to avoid the prediction offsets caused by high-order term losses.

The balance state evaluation results are combined with the internal connected battery cells of the lithium-ion battery pack by applying the battery difference in the calibration process, which can be applied to the calibration process, making the proposed algorithm to have a short calculation time and high calculation efficiency advantages. The cycling iterate calculation process includes time update and measurement update. The time update process is also called the prediction, which is a one-step prediction of the current state variable and provides a process of a priori estimation of the next time point. The calibration process is a feedback of the observations, which corrects the deviations at the same time as shown in Figure 1.

The basic parameters are important inputs to the associated battery management system device, such as voltage, current, and temperature. They are used to control and optimize the power flow both electrical loads and the distributed power sources. Wherein, the available power of the lithium-ion battery pack can be defined as an additional state in the iterate state-of-charge calculation process. In order to prevent the sudden voltage drop and current flow phenomenon, the outside parameters of the lithium-ion

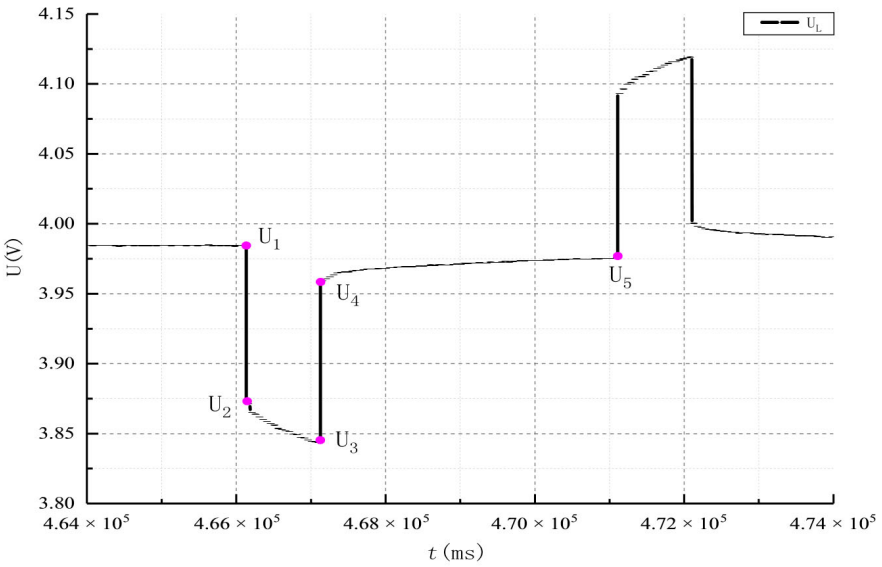

FIGURE 2 The Hybrid Pulse Power Characteristic test experimental procedure

battery pack should be detected in real-time and introduced into the state-of-charge estimation process, including closed-circuit voltage, battery cell voltage, and current. Prior to the overtaking maneuvers, the estimated state-of-charge value should be used to avoid the dangerous situations such as the sudden power outages that will lead to the critical dynamic conditions.

The adaptive state-of-charge estimation considers the current aging state and predicts the emergency due to its self-learning design characteristics, and its purpose is to react and predict the power demand of the power supply system immediately in the future. Extensive experiments have been conducted in advance to generate the dependency on the remaining available power of the lithium-ion battery pack in terms of battery states, voltages, and power pulse parameters. The operating current and temperature signals are measured and used as the input parameters of the state-of-charge estimation model, in which the different values of I are used for the working state amplification. In order to realize the energy management of the serially connected batteries, the battery management system is designed and implemented, in which the real-time temperature monitoring is achieved by the sensors fixed at the battery electrodes. The modular design of the overall structure is investigated by using the parameter matrix, together with the prediction and correction. Using the state variables as the output mode of the cache space, the effective state monitoring is realized by the observed data analysis. According to the basic principle analysis of the working process, it is suitable for the lithium-ion battery pack and the state-of-charge estimation is realized by the real-time monitoring.

The lithium-ion battery pack needs to be managed to ensure the safe operation in the emergency power supply process, in which the historical stored data can also provide a useful reference to its retirement. Considering the working characteristics of the lithium-ion battery pack, the heating and cooling plates are used to achieve the suitable operating temperature maintenance. In order to meet the online application requirements, the working state monitoring subsystem is also designed for the lithium-ion battery pack. The working condition monitoring and analysis are investigated to ensure application safety for the energy storage and supply process of the lithium-ion battery packs. The antijamming digital transmission signals can be obtained by the real-time signal monitoring in the battery management system. The security protection plays an important role in the lithium-ion battery packs, which is limited by the power supply due to its physical limitations. Experiments are carried out at different ambient temperatures by using the different discharge current rates, according to which the experimental data can be introduced into the discharge capacity calculation of the actual operating conditions.

3 | EXPERIMENTAL ANALYSIS

3.1 | Parameter identification

The parameter identification of the lithium-ion battery pack can be treated as a dynamic system, in which the direct application of the parameter identification submodule is designed and applied that is suitable for the power supply requirement. It has strong adaptability in realizing the time domain dynamic parameter relationship, the feature of which is obtained by using the dynamic mechanism of the recognition submodule. Therefore, the output value of the corresponding parameters can be effectively identified, in which the stabilization process is also implicit in the parameter identification. When the identification network is used, the defined recognition error function is introduced into the standard energy function. The target capture parameters of the lithium-ion battery

pack can be obtained by performing various pulse charge-discharge experiments, which are the encapsulation of the real-time closed-circuit voltage monitoring corresponding to different state-of-charge conditions. Then, an experimental calculation analysis is performed, and the variation law of the model coefficients can be calculated through the realization of the specific state-space equation. Finally, various model coefficients can be obtained and the overall working state description can be realized.

According to the parameter identification requirements of the state-space equation, the power battery test system was adopted (Company: YAKEYUAN; Channel number: 20; Voltage accuracy: 0.02%; Current accuracy: 0.02%; Temperature accuracy: 1°C). By using the intermittent Hybrid Pulse Power Characteristic test, the power characteristic experiments of various model parameters can be conducted, in which the variation law can be obtained. In order to obtain the closed-circuit voltage value in response to the open circuit voltage variation required for the lithium-ion battery pack, the constant current-constant voltage charging maintenance should be first applied fully to charge the lithium-ion battery pack with the state-of-charge value of 100%. In addition, it should be left for half an hour to stabilize its internal electrochemical reaction stable for the subsequent experimental test. In the experiment, a $0.2C_5A$ current is used to realize the intermittent cycling discharge. The experimental analysis is combined with the shelf phase, in which the discharge process was suspended after the CC discharge for 3 minutes. It is performed after a complete static operation for 40 minutes, after which the CC discharge and experimental test are conducted in accordance with the above process until the state-of-charge value is discharged to 0. The experimental test results of different time points in the intermittent charge-discharge test procedure are described in Figure 2.

In the above figure, U_1 is the initial discharge voltage value; U_2 is the initial discharge voltage, which is the battery instantaneous voltage value; U_3 is the discharge end voltage value; U_4 is the instantaneous voltage value after the battery is left for 40 seconds; and U_5 is the battery recovered voltage value after standing for 40 minutes.

Open circuit voltage: The open circuit voltage parameter of U_{OC} is the voltage across the battery of the positive and negative terminals for a long period of time. In order to obtain the open circuit voltage value of the lithium-ion battery corresponding to different state-of-charge states, the voltage is measured when state of charge = 1. And then, the battery is discharged at a constant current of 1 C for 6 minutes to reduce the state of charge by 0.1 and the battery is left for a long time. When the voltage reaches a steady state, the open circuit voltage value of the battery is measured again, and the cycle test is performed until the state of charge is lowered to zero.

Ohm resistance: When the discharge starts and the discharge stops, the polarization has not yet occurred. As a result, the battery terminal voltage sudden drop-and-rise phenomenon is caused by the ohmic internal resistance, in which the voltage transient process satisfies Ohm's law. Therefore, the ohmic internal resistance value can be calculated by Ohm's law. Aiming to improve the calculation accuracy of R_0, the average treatment of these two processes can be taken as the sample of R_0, the formula is shown in Equation (29).

$$R_0 = \frac{(U_1 - U_2) + (U_4 - U_3)}{2I} \tag{29}$$

Polarized internal resistance: When the battery is in a discharged state, the slow drop of the terminal voltage after the transient drop is due to the polarization internal resistance and the polarization capacitance. Since the battery is in a hold state before the discharge starts, the parallel resistance-capacitance portion can be regarded as a zero-state response within 10 seconds at the start time point of the discharge period, so the polarization internal resistance R_p can be identified according to the Equation (30).

$$\begin{cases} U_L = U_{OC} + IR_0 + U_p \\ U_p = IR_p\left(1 - e^{-t/\tau}\right) \end{cases} \tag{30}$$

In the formula, U_p is the voltage across the resistance-capacitance circuit loop. The battery has no external current flowing through the resistance-capacitance circuit for 40 seconds of the duration of the pulse after the end of the pulse discharge. At this time, the resistance-capacitance circuit can be regarded as a zero-input response, so the time constant τ can be calculated by the formula(31).

$$\tau = -\frac{t_4 - t_3}{\ln\left[(U_1 - U_5)/(U_1 - U_4)\right]} \tag{31}$$

Polarize capacitance: During the period from t_2 to t_3 where the battery is left after the end of the pulse discharge, due to the polarization effect, the induced current appears in the resistance-capacitance loop in the model, and the battery voltage will slowly rise. The time constant of the polarization reaction is $\tau = R_pC_p$, and its magnitude reflects the velocity of the transition process of the first-order resistance-capacitance circuit. As the calculation formula for τ is obtained together with the parameter value of R_p, C_p can be obtained as shown in Equation (32).

$$C_p = -\frac{t_4 - t_3}{R_p \ln\left[(U_1 - U_5)/(U_1 - U_4)\right]} \tag{32}$$

A 40-minute interval discharge is performed, and the Hybrid Pulse Power Characteristic test is performed at the end of the following 40-minute hold. During the intermittent discharge process, the embedded Hybrid Pulse Power

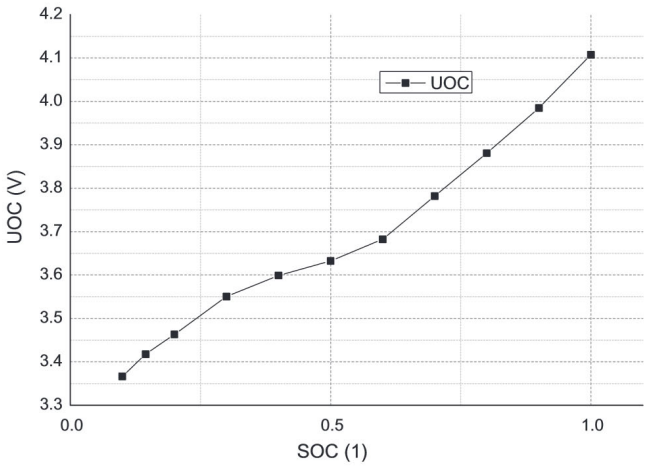

(A) open circuit voltage-state of charge

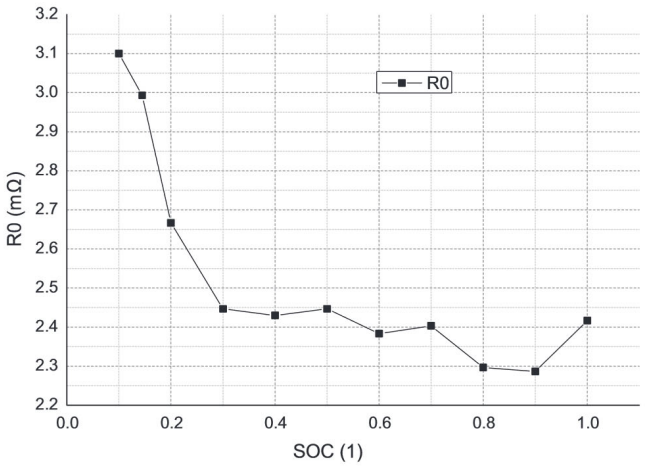

(B) Ohm resistance towards state of charge

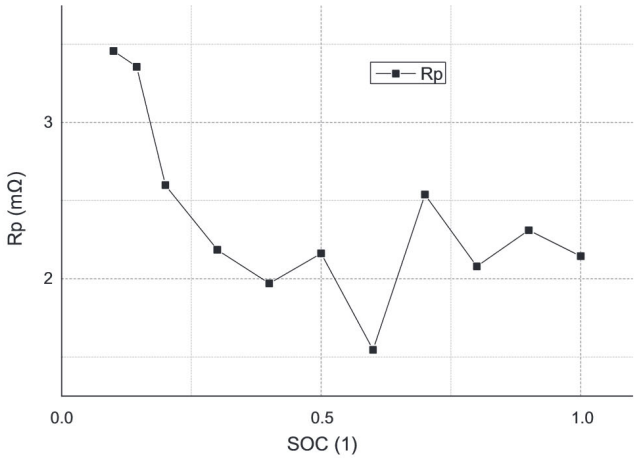

(C) Polarize resistance towards state of charge

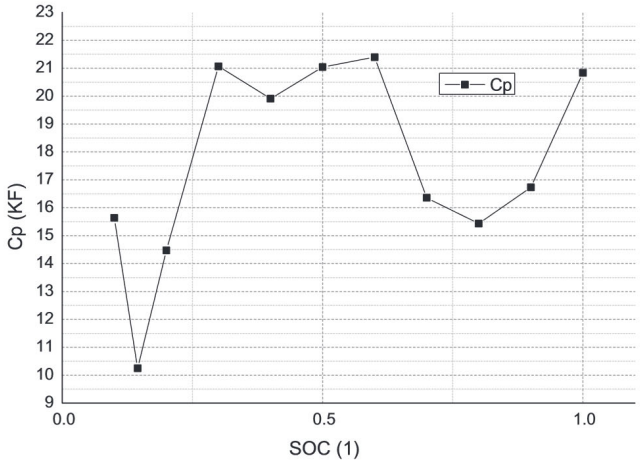

(D) Polarize capacitance towards state of charge

FIGURE 3 The parameter identification results. (A) open circuit voltage-state of charge. (B) Ohm resistance towards state of charge. (C) Polarize resistance towards state of charge. (D) Polarize capacitance towards state of charge

Characteristic test is performed at the end time point of the shelved time period, and then, the 5-seconds duration current pulse of each intermittent hold is set at the end time point of the shelved time period. According to the parameter identification purpose of the equivalent circuit model and its state-space equation structure, the experiment is performed at the room temperature based on the $1C_5A$ mixed pulse power characteristic test method. The dynamic characteristics can be obtained considering the different state-of-charge effects and the difference between the charge-discharge processes.

S1: A series of balanced charge processes are performed to make the lithium-ion battery pack full of energy, in which the fast CC charge is conducted in the phased array process, and then, the CV replenishment mode is turned on to make the state-of-charge value of each internal connected battery cell to be 100%. After leaving for 40 minutes, the Hybrid Pulse Power Characteristic test was performed and the data were recorded in real time.

S2: The 5.00% energy of the lithium-ion battery pack should be released for each state-of-charge state, in which the state-of-charge value drops to 95% at the first time and the Hybrid Pulse Power Characteristic test should be conducted at the end time point of the following shelved time period. In this way, it can be performed when the state-of-charge value equals to 100%, 95%, 90%, …, 10%, 5%, and 0. Subsequently, the equivalent model parameters can be obtained under the same state-of-charge conditions to identify the subsequent parameter identification process. If U_{OC} remains constant for a short time period, the closed-circuit voltage response to the corresponding lithium-ion battery pack is recorded with each current pulse. This cyclic current pulse is repeated for every 5% state-of-charge drop until the lithium-ion battery pack is fully discharged.

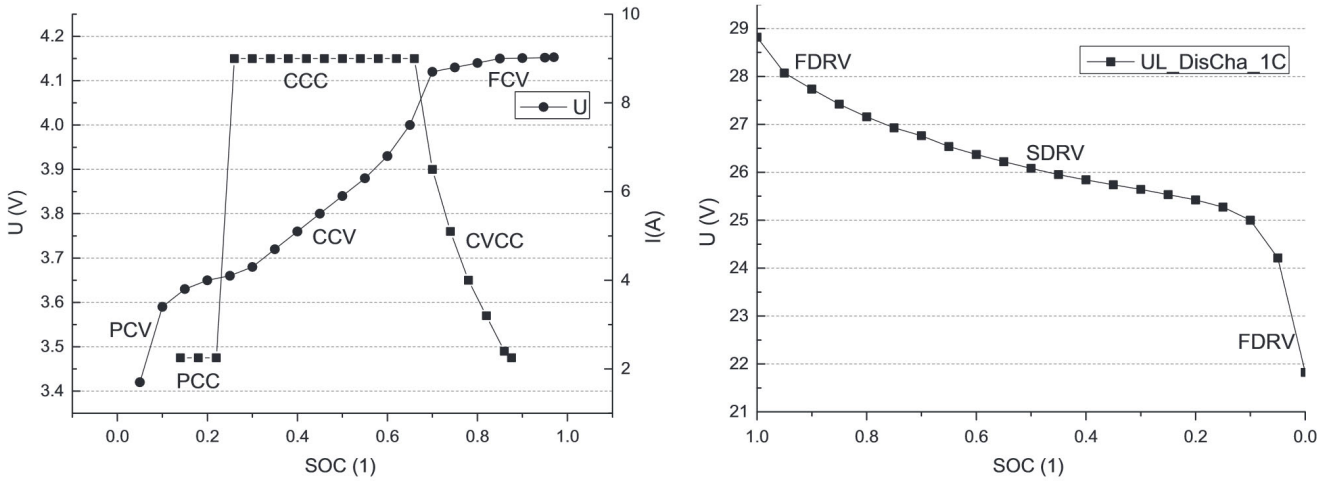

(A) Charge voltage and current

(B) CC discharge voltage characteristics

FIGURE 4 Working characteristics in the charge-discharge process. (A) Charge voltage and current. (B) CC discharge voltage characteristics

The closed-circuit voltage response is obtained by embedding the pulse charge-discharge process at different state-of-charge conditions, which is then used for its parameter identification. The coefficient of the functional equation can be obtained by integrating the closed-circuit voltage value of the lithium-ion battery pack. In addition, the functional relationship of the model parameters can be obtained by processing these coefficients. The parameter identification results are shown in Figure 3.

As it can be seen from the experimental results, unlike the ohmic internal resistance, when the ambient temperature is a constant value (20°C), the polarization internal resistance of the battery changes drastically with the state of charge. At the initial stage of discharge, R_p rises slightly. When the state of charge discharges to about 0.6, the polarization internal resistance drops to the minimum point. As the discharge progresses, the polarization internal resistance increases significantly. When the state of charge is <0.3, the internal parameters of the battery change greatly, which has a great relationship to the internal chemical reaction of the battery cells. As the near end, the electrochemical reaction against the battery changes drastically, resulting in the significant change of the battery terminal voltage.

3.2 | Charge-discharge characteristics

In the state-space function of the state-of-charge estimation model, the dynamic characteristics of the lithium-ion battery pack should be considered and the voltage and current can be represented by the nonlinear function of the dynamic real-time parameter monitoring. This approach helps to reduce the prior learning requirement, which has better generalization to adapt the variation. The basic part of the method is the adaptive structure, in which a difference function is applied to the adaptive state-of-charge estimation framework. As battery aging proceeds, the proposed iterate calculation method should be able to provide an accurate estimation of the remaining available power, which is a challenging problem. The voltage and current characteristics are analyzed in the charging process as shown in part (A) of Figure 4.

The parameters in Figure 4 are expressed as follows: precharge current (PCC), constant charge current (CCC), constant voltage charge current (CVCC), precharge voltage (PCV), and floating charge voltage (FCV). The voltage and current axes are used to characterize their variations in the constant current-constant voltage charging process. The PCC, CCC, and CVCC can be reflected in the current curve of the above figure. Finally, the auxiliary constant voltage charge process is performed in the last part of the charge process. During the charge process, the closed-circuit voltage does not change much and the current decreases accordingly. The reason for this phenomenon is that the electrical energy becomes full and the differential voltage value of the lithium-ion battery pack becomes smaller and smaller. It will be executed until the charge current is about to be the end-of-charge current (2.25A). Meanwhile, the charge voltage characteristics can be also reflected. As it can be known from Figure 4, the voltage increases rapidly from the CCC charge process. However, as the battery capacity is supplemented with the charge process, the voltage is essentially constant and the experiment will be stopped by the end-of-charge current limit.

The voltage drop rate is also different from the cross-current discharge process of different current rates, according to which the discharge voltage characteristics can be obtained and analyzed afterward. When the discharge voltage reaches the end-of-charge terminal voltage of 3.00 V, the discharge experiment will be terminated regardless of any environment. The working characteristics at different discharge current rates can be obtained finally by the

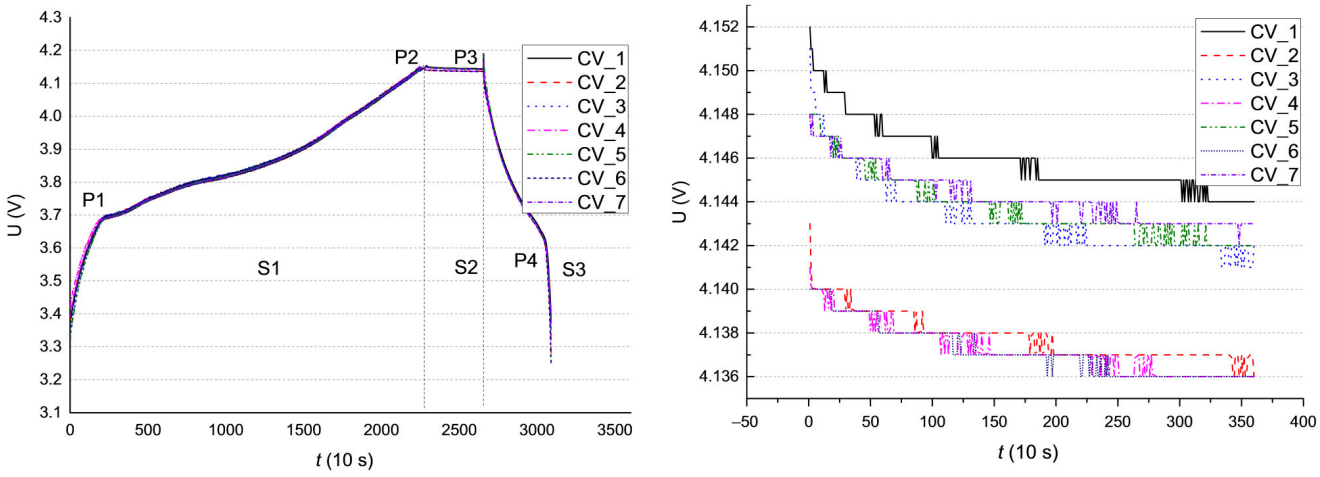

(A) Cell voltage variation during the cycling treatment

(B) Cell voltage characteristics in the shelved state

FIGURE 5 The cell voltage characteristics of the lithium-ion battery pack in the cycling charge-discharge process. (A) Cell voltage variation during the cycling treatment. (B) Cell voltage characteristics in the shelved state

experiments, forming the discharge voltage characteristic curve, which is shown in the part (B) of 0 and the parameters are shown as follows: fast dropping region voltage (FDRV) and slow dropping region voltage (SDRV). The battery voltage drops sharply along with the time extension of the first region, and the discharge voltage characteristics can be obtained accordingly. The discharge result is almost similar to the change law, in which the self-discharge process is also considered to represent the voltage difference. In the second region, the battery voltage decreases slowly over time. After entering the third zone, the battery voltage suddenly drops to the low voltage limit. Most of the working time is in the second area, and only a small part of the working time is in the first or third area. It is worth noting that this phenomenon satisfies the application requirements and the working length range of the second region, which is also an important health state indicator and plays a central role in the state-of-charge estimation. At different discharge current rates, the discharge time of the second region is also different.

3.3 | Cycling charge-discharge

The cycling charge-discharge experiments should be performed for the lithium-ion battery pack, in which 7 battery cells of 4 Ah capacities relate to series. Then, the charge (CC 9A/0.2C_5A to CV 4.15 V)-shelved-discharge (CC 45A/1C_5A) mode was used as one test cycle. Prior to the experiment, the previous discharge process was conducted for the lithium-ion battery pack and a time of 25°C was reserved. The charge process uses a constant current-constant voltage charge module: The charge current in the constant current mode is 9.0A, and it converts to constant voltage mode charge when the battery cell voltage reaches the high voltage of 4.15 V. The discharge process uses a large current discharge method, in which the constant current series discharge can be investigated until the entire lithium-ion battery pack voltage drops to 21 V or the battery cell voltage drops to 3.0 V. The cycling charge-discharge experiments repeat and the experimental data can be measured together with the accompanying restorage.

A single charge-discharge curve of the lithium-ion battery pack is shown in part (A) of Figure 5, in which the trend curve of the lithium-ion battery pack is the same as the single one battery cell in the charge-discharge process. The working state of the lithium-ion battery pack appears in these three stages. The charge rate of the lithium-ion battery pack is slower than the single battery cell. Because of the polarization of the shelf, the single battery cell voltage has a constant ice base battery voltage. When this part has up and down floats and standards, there should be more time. During the discharge process, it is obvious that the early stage of the relatively fixed closed-circuit voltage and the stable discharge are changed, making it tends to be slow. As a result, the discharge rate of the single battery cell is relatively slow in the discharge process and the discharge time is long as well, in which the conversion process is a single turret corresponding to a small lag for two hours. The experimental results show that the lithium-ion battery pack has special feature of the single battery cell, and the operational features of the lithium-ion battery pack are different from a single battery cell.

The lithium-ion battery pack is placed in a static state at 25°C for approximately four hours at room temperature to restore temperature and activity to a steady state, during which the electrical parameters are monitored to obtain the boundary

TABLE 1 Charge-discharge parameters with different current ratio

Name	Group 1	Group 2	Group 3	Group 4	Group 5
Charge rate	0.50C	0.20C	0.30C	1.00C	1.20C
Discharge rate	1.00C	0.50C	0.20C	1.20C	0.30C

TABLE 2 Charging efficiency at different current rates

Name	Group 1	Group 2	Group 3	Group 4	Group 5
Charge rate	0.50C	0.20C	0.30C	1.00C	1.20C
Power	3.5861	3.7599	3.7217	3.3844	3.2307
Efficiency	0.9548	1.0000	0.9894	0.9001	0.8590

TABLE 3 Coefficient relation of charging efficiency and current ratio

Name	p_1	p_2	p_3	p_4	p_5
Value	−0.6462	1.6850	−1.4630	0.3471	0.9766

voltage variations and capacities that are shown in part (B) of 0. As it is shown in part (B) of Figure 5, there is a significant battery difference when the lithium-ion battery pack is placed on hold. During the shelving process, the self-discharge rate of each battery is varied, due to the discharge current rate difference between each battery cells. However, compared to the other two phases, this difference phenomenon is too small to be calculated in the state-of-charge estimation process. The operating characteristics often cause the over-discharge disks on the lithium-ion battery pack. Unlike other type of batteries, it can be restored automatically, which will cause permanent damage. Therefore, the self-discharge rate and battery inconsistency have a significant impact on the state-of-charge estimation process of the entire lithium-ion battery pack.

3.4 | Current rate correction

Aiming to improve the adaptability of the proposed method, the different current rate experiments are designed for the coulomb efficiency calculation during the different current charge-discharge maintenance process, which are investigated in the correction step of the iterate calculation process. By conducting the varying current test, the correction factors are obtained and taken into the optimization treatment, including the temperature influence on the polarization resistance. The current rates for charging and discharging experimental process are shown in Table 1.

As can be known from the analysis of the experimental results, the efficiency decreases as the charging rate increases. Therefore, the relative capacity ratio of different charge rates, that is, the charge efficiency, is obtained by using the 0.20 C charging current rate, and the calculation expression thereof is shown in Equation (33).

$$\eta_c = \frac{Cx}{C_{0.20}}, x = 0.50, 0.20, 0.30, 1.00, 1.20 \quad (33)$$

In addition, the charging efficiency η at different current rates can be obtained according to the experimental results, which are shown in Table 2.

Since it is not easy to observe the change law of charge efficiency directly from the data, it is not easy to obtain the charge efficiency function relationship of the above table. Therefore, the variation law of the charging efficiency can be more intuitively described by drawing the curve, and then, the charging efficiency curve can be obtained under different charging rates.[52] As a result, a positive correlation between the charging efficiency and charging current rate can be obtained. By comparing and analyzing the function fitting effects on different orders, the fourth-order polynomial fitting method is selected as the fitting function relationship, and the calculation expression is shown in Equation (34).

$$\eta_c = f(x) = p_1 * x^4 + p_2 * x^3 + p_3 * x^2 + p_4 * x^1 + p_5 \quad (34)$$

In the above Equation, x is the current rate, ηc is the efficiency, and p_1 to p_5 are the coefficients of the respective subitems. Then, the coefficient value of each subitem is obtained by a curve fitting function. In the above functional relation expression, the coefficient values of various items are shown in Table 3.

In order to achieve the purpose of fitting the coefficient function, the corresponding polarization capacitance values of different state of charge are calculated by using the functional relation expression. The experimental results are compared with the original collected data, and the tracking effect of the fitting curve is verified. Finally, the variation on the coulomb efficiency can be obtained. The results show that the fitting equation has a good effect on the simulation of the running characteristic of the airborne lithium-ion battery pack s. By embedding the charging efficiency in the state-of-charge prediction process, the prediction accuracy of the airborne lithium-ion battery pack can be improved on the charging and discharging process.[53] In order to calculate the coulomb efficiency of different current charging and discharging processes, simulated working condition experiments are designed with different charging and discharging rates. The experimental parameters of different current rates are set that is shown in Table 4.

TABLE 4 Discharge experimental parameters list with different current ratio

Name	Group 1	Group 2	Group 3	Group 4	Group 5	Group 6
Charge rate	1.00C	1.00C	1.00C	1.00C	1.00C	1.00C
Discharge rate	0.10C	1.00C	0.50C	0.20C	1.20C	0.30C

At a charge rate of $0.10C_5A$, the discharge efficiency is the highest, and as the discharge rate increases, the discharge efficiency gradually decreases. Therefore, the relative capacity ratio of different discharge rates can be obtained with a 0.10C discharge rate. The discharge efficiency is obtained, and the calculation formula is shown in Equation (35).

$$\eta_d = \frac{Cx}{C_{0.10}}, x = 0.10, 0.50, 0.20, 0.30, 1.00, 1.20 \quad (35)$$

In addition, the charging efficiency η at different current rates can be obtained according to the experimental results that are shown in Table 5.

It is difficult to observe the functional relationship directly from the data onto the table. Therefore, using the experimental results of the table, according to the positive correlation between the discharge efficiency and the discharge rate, the curve is drawn to more intuitively describing the variation law of the discharge efficiency. By comparing and analyzing the function fitting effect on different orders, the third-order polynomial function is selected as the fitting function relationship, and the calculation expression is shown in Equation (36).

$$\eta_d = f(x) = p_1 * x^3 + p_2 * x^2 + p_3 * x^1 + p_4 \quad (36)$$

In the above Equation, x represents the discharge current multiplication factor, and the coefficient values of the various items are shown in Table 6.

In the calculation process, the purpose of coefficient effected verification and the functional relation expression after function fitting treatment is applied, obtaining the corresponding coulomb efficiency values under different current multiplication rates. This can be compared to the original collected data to verify the tracking effect of the fitted curve. The fitting equation has a good effect on the simulation of the running characteristic of the airborne lithium-ion battery pack. By embedding the discharge efficiency in the state-of-charge prediction process, the state-of-charge prediction accuracy of the airborne lithium-ion battery pack is improved on the charging and discharging experiments.

3.5 | State estimation effect

The lithium-ion battery pack is mainly used for the instrument inspection and other emergency power supply purposes of the aircraft flying conditions. Taking the lithium-ion battery pack as the research object, the voltage variation law and the voltage difference between the battery cells are studied by designing the simulated various working condition experiments. When the change rate of the operating condition is large, the closed-circuit voltage change rate and the battery voltage will be obvious. The voltage difference is as high as 120 mV, but the different operating effect is relatively small on the battery voltage difference.

The experimental procedure is designed as follows.

S1: It should be determined whether the single battery voltage and closed-circuit voltage are greater than the minimum voltages 3 V and 21 V, and it will enter the second experimental step when the closed-circuit voltage or battery voltage meets the conditions. Otherwise, it will jump to the tenth step.
S2: The lithium-ion battery pack should be left shelved for 10 seconds and turned to the third step.
S3: A $0.30C_5A$ discharge is performed while the real-time voltage monitoring is set up to determine whether the battery cell voltage and closed-circuit voltage are greater than the minimum voltage limitation. The experimental procedure will be turned to the fourth step under the satisfactory conditions, or jump into the tenth step.
S4: The ignition simulation with $0.60C_5A$ discharging treatment should be maintained for B seconds, and it should be determined whether the battery cell voltage and closed-circuit voltage are greater than the minimum voltage limitation. If the condition is met, the fifth step should be entered; otherwise, the experimental procedure will skip to the tenth step.
S5: The lithium-ion battery pack should be charged with a current of $0.10C_5A$ for C seconds to obtain the analog supplemental power supply process and turned into the sixth step.

TABLE 5 Efficiency at different current rate discharges

Name	Group 1	Group 2	Group 3	Group 4	Group 5	Group 6
Rate	0.10	1.00	0.50	0.20	1.20	0.30
Energy	3.4063	3.3560	3.3716	3.3941	3.3500	3.3831
Efficiency	1.0000	0.9852	0.9898	0.9964	0.9835	0.9932

S6: The self-discharge characteristics can be simulated by conducting the 0.01 C_5A cycling discharge process for D seconds, and then, the experimental procedure will proceed with the seventh step.
S7: The 0.10 C_5A charge process can be investigated by performing C seconds analog replenishment power and proceed to step 8.
S8: The emergency output can be simulated by the 1C_5A discharge current for E seconds, and the battery management system determines whether the battery voltage and closed-circuit voltage are greater than the minimum voltage limitation in real time. When the voltage meets the requirements of the experimental conditions, the experimental procedure should go to the ninth step. Otherwise, the experimental procedure should jump into the tenth step.
S9: The experimental test should repeat steps from 2 to 8 until the conditions are not met and jump to tenth step.
S10: The end. T_a is the discharge time of the instrument inspection step, 50 seconds. T_b is the aircraft ignition discharge time, 5 seconds. T_c is the recharge time, 20 seconds. T_d is the self-discharge time, 10 seconds. T_e characterizes the emergency power supply time, 30 seconds.

External direct monitoring signals of the lithium-ion battery pack during the experiment can be obtained by real-time monitoring. These signals are input into the state-of-charge estimation model, and a closed-circuit voltage tracking signal can be obtained. The closed-circuit voltage tracking effect along with the current variation can be obtained, which is shown in Figure 6, in which U_1 and U_2 represent the closed-circuit voltage data obtained by the real-time sampling and the calculation toward time during the state-of-charge estimation process. As it can be shown from the graphical experimental result analysis, the proposed method can achieve effective closed-circuit voltage tracking. The estimated error is 1.00%, which indicates that the closed-circuit voltage tracking has good estimation effect on the main discharge simulation condition. Meanwhile, the state-of-charge estimation analyzed that is shown in the right part of Figure 6, in which the *state of charge*$_1$ integral is obtained by the Ah integration algorithm, and the proposed method is used to implement state of charge$_2$. The experimental results show that the proposed method has a good effect on the online state-of-charge estimation toward the hour integral integration method by analyzing the experimental results in the complex current working conditions. Experimental results show that this novel weight coefficient calculation method can improve the state estimation accuracy. The state-of-charge value calculated by Ah integration has a significant systematic error because of the accumulation, and the weight coefficient calculation can be corrected to the zero return.

The MMSE evaluation method is used to verify the applicability of the joint state-of-charge estimation algorithm, in which the estimation effects on different initial state-of-charge values are analyzed. The energy and time efficiency[54] were utilized to improve battery uniformity with the group working lithium-ion battery pack. In addition, it has higher accuracy in various modes, compared to the state-of-charge estimation results[53] with better converge. When the initial state-of-charge value of the constructed filter is close to the actual value, the state-of-charge

TABLE 6 Fitting coefficient of current efficiency and ratio

Name	p_1	p_2	p_3	p_4
Value	−0.01828	0.04852	−0.04936	1.004

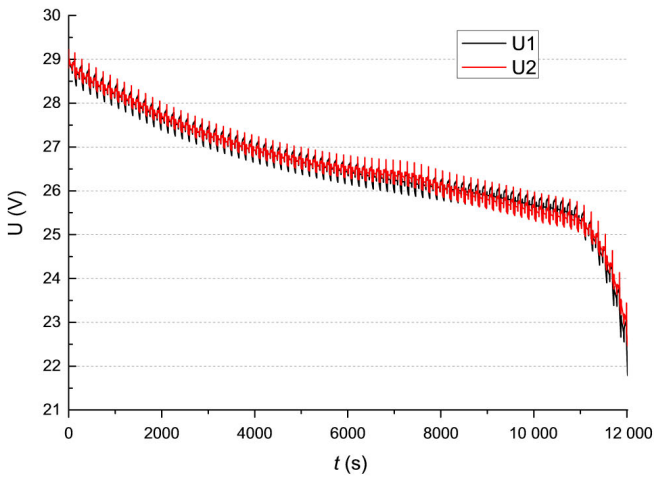

(A) closed-circuit voltage changing law

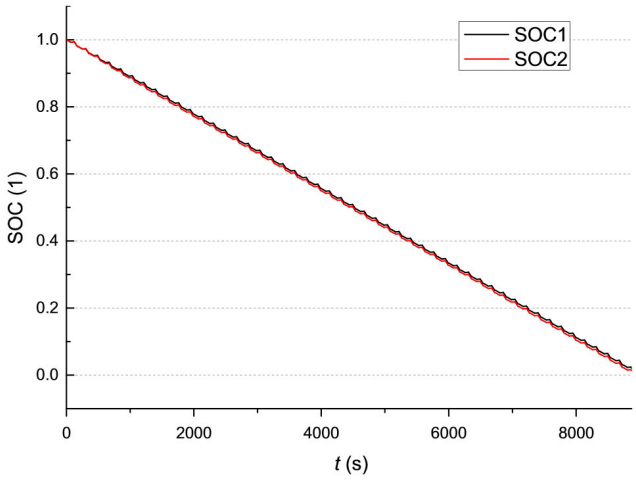

(B) state of charge estimation effect

FIGURE 6 The closed-circuit voltage changing law and the state-of-charge estimation effect. (A) closed-circuit voltage changing law. (B) state-of-charge estimation effect

TABLE 7 BBDST working condition parameters and description

Ph (kw)	Pc (w)	Single step (s)	Grand total (s)	Working condition	37.5	69	21	134	Accelerate
37.5	69	21	21	Start	4.5	9	16	150	Sliding
72.5	135	12	33	Accelerate	−15	−27	6	156	Brake
4.5	9	16	49	Sliding	72.5	135	9	165	Accelerate
−15	−27	6	55	Brake	92.5	174	6	171	Rapid acceleration
37.5	69	21	76	Accelerate	37.5	69	21	192	Accelerate
4.5	9	16	92	Sliding	4.5	9	16	208	Sliding
−15	−27	6	98	Brake	−35	−66	9	217	Brake
72.5	135	9	107	Accelerate	−15	−27	6	229	Brake
92.5	174	6	113	Rapid acceleration	4.5	9	71	300	Parking

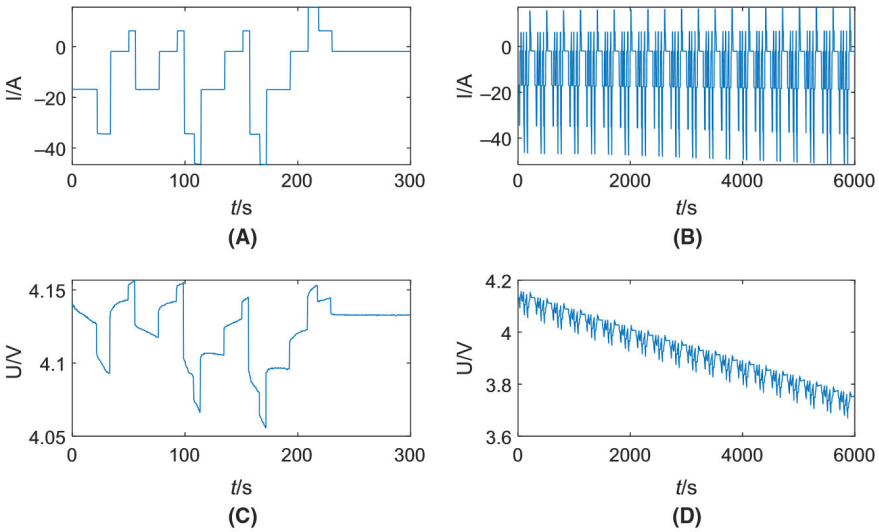

FIGURE 7 BBDST working condition experimental data

estimation of the lithium-ion battery pack is compared by three model-based algorithms in a new combined dynamic loading profile,[55] where the estimated results had similar experimental values compared to the experimental results obtained in this research. In addition, the correctness and accuracy of the proposed estimation model can be verified by the experimental results. The actual initial value will be corrected in the state-of-charge estimation process, in which the jitter is negligible. The superposition efficiency is analyzed under the complex current variation working conditions, which reflects that the proposed method can realize the effective state-of-charge estimation. In addition, the experimental results show that the developed battery management system device has good influence on the lithium-ion battery pack energy supply process.

3.6 | Complex condition analysis

Refer to the Beijing bus dynamic stress test (BBDST) setting working condition test to test the used lithium battery LFP50AH ternary lithium battery. Battery charging and discharging equipment The BTS750-200-100-4 battery testing equipment provided by Shenzhen Yakeyuan Technology Co., Ltd. sets the steps according to the data in Table 7 and conducts experiments.

The BBDST working condition is the actual data acquisition of the Beijing bus. In Table 7, Ph (kW) is the actual battery output power under the conditions of the bus start acceleration and taxiing. Since the experiment was carried out on the battery of 50 Ah, the data in Pc(w) were obtained by reducing Ph(kw), and Pc(w) was used for the experiment of the LFP50Ah ternary lithium battery of China National Aviation Corporation. As can be seen from the data table, the time of a complete BBDST is 300 seconds, and the BBDST condition test is performed 20 times on the battery, and the BBDST condition data can be obtained as shown in Figure 7.

In Figure 7, (A) and (C) are the experimental current and voltage data of the first BBDST condition, and (B) and (D) are the experimental current and voltage data of 20 BBDST conditions, respectively. Since the BBDST operating condition is power discharge, it can be seen from (B) and (D) that the discharge current increases and the battery terminal voltage shows a downward trend when the number of cycles

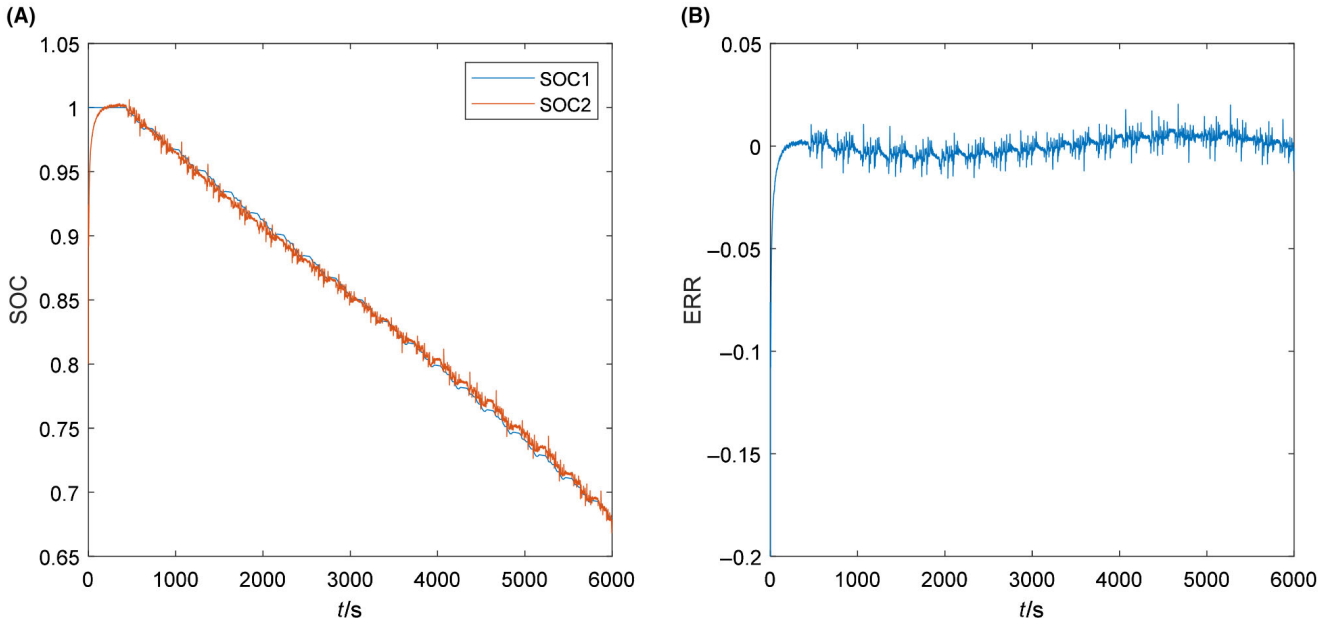

FIGURE 8 State-of-charge estimation result and error curve

increases. The equivalent circuit model was established by parameter identification of HPPC experimental data. In order to verify the validity of the model, the model data and actual data were compared and analyzed with additional battery operating conditions data. The model was verified by the BBDSTT condition, and the various working conditions of the battery were simulated by constant power discharge for a certain period. The test device obtains the current value in the experimental data as the input condition, and the simulated terminal voltage is compared with the experimental acquisition terminal voltage by the simulation model. According to the established resistance-capacitance equivalent circuit model and the extended Kalman algorithm, the state-of-charge estimation of the BBDSTT condition is carried out. The error between the initial value and the true value is given at least 20% in advance, so that the state-of-charge estimation is performed, and the obtained result is shown in Figure 8.

In Figure 8, (A) is a graph of estimation results, SOC1 is a true state-of-charge value, and SOC2 is a state-of-charge estimation value using an extended Kalman algorithm. (B) is an error curve obtained by subtracting two state-of-charge value curves. The state-of-charge estimation error based on the established resistance-capacitance model using improved extended Kalman filter algorithm is <2.00%. It can correct the error of the initial value very well, which does not depend on the accuracy of the initial value and has a strong correction function.

4 | CONCLUSIONS

An adaptive weight coefficient calculation incorporates the state-of-charge estimation of the lithium-ion battery pack, in which the weight coefficient is fully applicable to the online working state monitoring by establishing a suitable environment. By implying a new weighting factor calculation method, it achieves the accurate working state monitoring purpose, in which the improved weight coefficient calculation treatment is introduced and its numerical stability is improved. The recursive calculation is derived by using the real-time detected parameters, aiming to adapt the complex current variation working conditions. In addition, the nonlinear treatment is used to construct the unscented transform function, according to which a novel state-of-charge estimation model is investigated by using the iterative calculation process and provides a theoretical basis for the energy-based cleaner production. The complex current variation working condition capability is verified by conducting the experimental tests, and the coefficient correction processing of the adaptive calculation realizes the accurate working state monitoring of the power supply in the lithium-ion battery pack. Meanwhile, as the calculation requirement is small, the algorithm realization is easier compared to the power security protection process of the lithium-ion battery pack. As the proposed weight coefficient calculation method is quite effective in the real-time state monitoring of the lithium-ion battery packs under complex current variation situations, it will be applied to the battery management system exploratorily for performance testing and further improvement under different working conditions.

ACKNOWLEDGMENTS

This research was supported by National Natural Science Foundation of China (No. 61801407), China Scholarship

Council (No. 201908515099), Sichuan Province Science and Technology Support Program (No. 19ZDYF1098, 2019JDTD0019, 2019YFG0427, 2018GZ0390), Scientific Research Fund of Sichuan (No. 17ZB0453), and Teaching Research Project (18lzx665, 18gjzx11, 18xnsu12). Thanks to the sponsors.

ORCID

Shun-Li Wang https://orcid.org/0000-0003-0485-8082

REFERENCES

1. Noelle DJ, Shi Y, Wang M, Le AV, Qiao YU. Aggressive electrolyte poisons and multifunctional fluids comprised of diols and diamines for emergency shutdown of lithium-ion batteries. *J Power Sources*. 2018;384:93-97.
2. Wang YJ, Zhang CB, Chen ZH. A method for joint estimation of state-of-charge and available energy of LiFePO4 batteries. *Appl Energy*. 2014;135:81-87.
3. Wang YJ, Zhang CB, Chen ZH. A method for state-of-charge estimation of LiFePO4 batteries at dynamic currents and temperatures using particle filter. *J Power Sources*. 2015;279:306-311.
4. Burgos-Mellado C, Orchard ME, Kazerani M, Cárdenas R, Sáez D. Particle-filtering-based estimation of maximum available power state in Lithium-Ion batteries. *Appl Energy*. 2016;161:349-363.
5. Abu Qahouq JA, Xia ZY. Single-perturbation-cycle online battery impedance spectrum measurement method with closed-loop control of power converter. *IEEE Trans Industr Electron*. 2017;64(9):7019-7029.
6. Chen Y, Liu X, Cui Y, Zou J, Yang S. A multiwinding transformer cell-to-cell active equalization method for lithium-ion batteries with reduced number of driving circuits. *IEEE Trans Power Electron*. 2016;31(7):4916-4929.
7. Wu W, Wu W, Qiu X, Wang S. Low-temperature reversible capacity loss and aging mechanism in lithium-ion batteries for different discharge profiles. *Int J Energy Res*. 2019;43(1):243-253.
8. Cabañero MA, Boaretto N, Röder M, Müller J, Kallo J, Latz A. Direct Determination of Diffusion Coefficients in Commercial Li-Ion Batteries. *J Electrochem Soc*. 2018;165(5):A847-A855.
9. Zheng Y, Gao W, Ouyang M, Lu L, Zhou L, Han X. State-of-charge inconsistency estimation of lithium-ion battery pack using mean-difference model and extended Kalman filter. *J Power Sources*. 2018;383:50-58.
10. Zheng L, Zhu J, Lu D-C, Wang G, He T. Incremental capacity analysis and differential voltage analysis based state of charge and capacity estimation for lithium-ion batteries. *Energy*. 2018;150:759-769.
11. Zhang XU, Wang Y, Wu JI, Chen Z. A novel method for lithium-ion battery state of energy and state of power estimation based on multi-time-scale filter. *Appl Energy*. 2018;216:442-451.
12. Wang S, Fernandez C, Liu X, Su J, Xie Y. The parameter identification method study of the splice equivalent circuit model for the aerial lithium-ion battery pack. *Measure Cont*. 2018;51(5–6):125-137.
13. Wang YJ, Zhang CB, Chen ZH. A method for state-of-charge estimation of Li-ion batteries based on multi-model switching strategy. *Appl Energy*. 2015;137:427-434.
14. Fuengwarodsakul NH. Battery management system with active inrush current control for Li-ion battery in light electric vehicles. *Electr Eng*. 2016;98(1):17-27.
15. Hussein AA, Fardoun AA, Stephen SS. An online frequency tracking algorithm using terminal voltage spectroscopy for battery optimal charging. *IEEE Trans Sustain Energy*. 2016;7(1):32-40.
16. Ju F, Deng WW, Li JS. Performance evaluation of modularized global equalization system for lithium-ion battery packs. *IEEE Trans Autom Sci Eng*. 2016;13(2):986-996.
17. Li J, Wang L, Lyu C, Wang H, Liu X. New method for parameter estimation of an electrochemical-thermal coupling model for LiCoO2 battery. *J Power Sources*. 2016;307:220-230.
18. Lim KaiChin, Bastawrous HA, Duong V-H, See KW, Zhang P, Dou SX. Fading Kalman filter-based real-time state of charge estimation in LiFePO4 battery-powered electric vehicles. *Appl Energy*. 2016;169:40-48.
19. Lin C, Mu H, Xiong R, Shen W. A novel multi-model probability battery state of charge estimation approach for electric vehicles using H-infinity algorithm. *Appl Energy*. 2016;166:76-83.
20. Liu C, Liu W, Wang L, Hu G, Ma L, Ren B. A new method of modeling and state of charge estimation of the battery. *J Power Sources*. 2016;320:1-12.
21. Mohan S, Kim Y, Stefanopoulou AG. Energy-conscious warm-up of li-ion cells from subzero temperatures. *IEEE Trans Industr Electron*. 2016;63(5):2954-2964.
22. Su L, Zhang J, Huang J, et al. Path dependence of lithium ion cells aging under storage conditions. *J Power Sources*. 2016;315:35-46.
23. Sturm J, Ennifar H, Erhard SV, Rheinfeld A, Kosch S, Jossen A. State estimation of lithium-ion cells using a physicochemical model based extended Kalman filter. *Appl Energy*. 2018;223:103-123.
24. Sarasketa-Zabala E, Martinez-Laserna E, Berecibar M, Gandiaga I, Rodriguez-Martinez LM, Villarreal I. Realistic lifetime prediction approach for Li-ion batteries. *Appl Energy*. 2016;162:839-852.
25. Shi W, Wang J, Zheng J, Jiang J, Viswanathan V, Zhang J-G. Influence of memory effect on the state-of-charge estimation of large format Li-ion batteries based on LiFePO4 cathode. *J Power Sources*. 2016;312:55-59.
26. Li K, Wei F, Tseng KJ, Soong B-H. A Practical Lithium-Ion Battery Model for State of Energy and Voltage Responses Prediction Incorporating Temperature and Ageing Effects. *IEEE Trans Industr Electron*. 2018;65(8):6696-6708.
27. Xie JL, Ma JC, Bai K. State-of-charge estimators considering temperature effect, hysteresis potential, and thermal evolution for LiFePO4 batteries. *Int J Energy Res*. 2018;42(8):2710-2727.
28. Mao C, An SJ, Meyer HM, et al. Balancing formation time and electrochemical performance of high energy lithium-ion batteries. *J Power Sources*. 2018;402:107-115.
29. Zhang C, Allafi W, Dinh Q, Ascencio P, Marco J. Online estimation of battery equivalent circuit model parameters and state of charge using decoupled least squares technique. *Energy*. 2018;142:678-688.
30. Wang S, Fernandez C, Chen M, Wang LU, Su J. A novel safety anticipation estimation method for the aerial lithium-ion battery pack based on the real-time detection and filtering. *J Clean Prod*. 2018;185:187-197.
31. Ye M, Guo H, Xiong R, Yu Q. A double-scale and adaptive particle filter-based online parameter and state of charge estimation method for lithium-ion batteries. *Energy*. 2018;144:789-799.

32. Shen YQ. Improved chaos genetic algorithm based state of charge determination for lithium batteries in electric vehicles. *Energy*. 2018;152:576-585.
33. Wang YJ, Sun ZD, Chen ZH. Development of energy management system based on a rule-based power distribution strategy for hybrid power sources. *Energy*. 2019;175:1055-1066.
34. Xie J, Ma J, Sun Y, Li Z. Estimating the state-of-charge of lithium-ion batteries using an h-infinity observer with consideration of the hysteresis characteristic. *J Power Electron*. 2016;16(2):643-653.
35. Wang Y, Liu C, Pan R, Chen Z. Modeling and state-of-charge prediction of lithium-ion battery and ultracapacitor hybrids with a co-estimator. *Energy*. 2017;121:739-750.
36. Xia B, Mi C. A fault-tolerant voltage measurement method for series connected battery packs. *J Power Sources*. 2016;308:83-96.
37. Xie Q, Kim Y, Wang Y, Kim J, Chang N, Pedram M. Principles and efficient implementation of charge replacement in hybrid electrical energy storage systems. *IEEE Trans Power Electron*. 2014;29(11):6110-6123.
38. Xu Y, Li Z, Zhao J, Zhang J. Distributed robust control strategy of grid-connected inverters for energy storage systems' state-of-charge balancing. *IEEE Trans Smart Grid*. 2018;9(6):5907-5917.
39. Yang F, Wang D, Zhao Y, Tsui K-L, Bae SJ. A study of the relationship between coulombic efficiency and capacity degradation of commercial lithium-ion batteries. *Energy*. 2018;145:486-495.
40. Yang D, Zhang XU, Pan R, Wang Y, Chen Z. A novel Gaussian process regression model for state-of-health estimation of lithium-ion battery using charging curve. *J Power Sources*. 2018;384:387-395.
41. Wang Y, Yang D, Zhang XU, Chen Z. Probability based remaining capacity estimation using data-driven and neural network model. *J Power Sources*. 2016;315:199-208.
42. Xu X, Li ZG, Chen N. A Hierarchical Model for Lithium-Ion Battery Degradation Prediction. *IEEE Trans Reliab*. 2016;65(1):310-325.
43. Yan W, Zhang B, Wang X, Dou W, Wang J. Lebesgue-sampling-based diagnosis and prognosis for lithium-ion batteries. *IEEE Trans Industr Electron*. 2016;63(3):1804-1812.
44. Xiong R, Li L, Li Z, Yu Q, Mu H. An electrochemical model based degradation state identification method of Lithium-ion battery for all-climate electric vehicles application. *Appl Energy*. 2018;219:264-275.
45. Zhou D, Zhang KE, Ravey A, Gao F, Miraoui A. Online estimation of lithium polymer batteries state-of-charge using particle filter-based data fusion with multimodels approach. *IEEE Trans Ind Appl*. 2016;52(3):2582-2595.
46. Pugalenthi K, Raghavan N. A holistic comparison of the different resampling algorithms for particle filter based prognosis using lithium ion batteries as a case study. *Microelectron Reliab*. 2018;91:160-169.
47. Zou Y, Li SE, Shao B, Wang B. State-space model with non-integer order derivatives for lithium-ion battery. *Appl Energy*. 2016;161:330-336.
48. Zhao Y, Stein P, Bai Y, Al-Siraj M, Yang Y, Xu B-X. A review on modeling of electro-chemo-mechanics in lithium-ion batteries. *J Power Sources*. 2019;413:259-283.
49. Xiong R, Tian J, Shen W, Sun F. A novel fractional order model for state of charge estimation in lithium ion batteries. *IEEE Trans Veh Technol*. 2019;68(5):4130-4139.
50. Zelger C, Süßenbacher M, Laskos A, Gollas B. State of charge indicators for alkaline zinc-air redox flow batteries. *J Power Sources*. 2019;424:76-81.
51. Yang F, Li W, Li C, Miao Q. State-of-charge estimation of lithium-ion batteries based on gated recurrent neural network. *Energy*. 2019;175:66-75.
52. Afshari HH, Attari M, Ahmed R, Delbari A, Habibi S, Shoa T. Reliable state of charge and state of health estimation using the smooth variable structure filter. *Cont Eng Pract*. 2018;77:1-14.
53. Li GD, Peng K, Li B. State-of-charge Estimation for Lithium-ion Battery using a Combined Method. *J Power Electron*. 2018;18(1):129-136.
54. Li S, Hu M, Li Y, Gong C. Fractional-order modeling and SOC estimation of lithium-ion battery considering capacity loss. *Int J Energy Res*. 2019;43(1):417-429.
55. Morstyn T, Savkin AV, Hredzak B, Agelidis VG. Multi-agent sliding mode control for state of charge balancing between battery energy storage systems distributed in a DC Microgrid. *IEEE Trans Smart Grid*. 2018;9(5):4735-4743.

How to cite this article: Wang S-L, Fernandez C, Xie Z-W, Li X-X, Zou C-Y, Li Q. A novel weight coefficient calculation method for the real-time state monitoring of the lithium-ion battery packs under the complex current variation working conditions. *Energy Sci Eng*. 2019;7:3038–3057. https://doi.org/10.1002/ese3.478